Laser–tissue interaction modeling with LATIS

R. A. London, M. E. Glinsky, G. B. Zimmerman, D. S. Bailey, D. C. Eder, and S. L. Jacques

The role of modeling in designing new treatment protocols and instruments is discussed. A computer program for modeling laser–tissue interaction named LATIS is described. Interactions are divided into the processes of laser propagation, thermal effects, material effects, and hydrodynamics. Full coupling of the processes is taken into consideration. Applications in photothermal and photomechanical laser–tissue interactions are briefly discussed. A detailed description is given of a particular application of LATIS to study the effects of dynamic optical properties on dosimetry in photothermal therapy. Optical properties are functions of tissue damage, as determined by previous measurements. Results are presented for the time variation of the light distribution and damage within the tissue as the optical properties of the tissue are altered. It is found that proper accounting of dynamical optical properties is important for accurate dosimetry modeling. © 1997 Optical Society of America

Key words: Laser–tissue modeling, dynamic optics, laser dosimetry, tissue damage.

1. Introduction

The development of new instruments and procedures for use in laser medicine typically involves extensive experimental and clinical studies. Computational modeling of the laser–tissue interaction process can be used to explore and reduce the experimental parameter space (e.g., laser wavelength, pulse length, and pulse energy) and to gain a deeper understanding of specific laser-medical processes. In this way, modeling can lead to more rapid development and to the genesis of new ideas. In addition, modeling will be useful in the future for patient-specific treatment planning and for physician training. A project to develop a specific instrument or procedure will generally involve iteration between modeling and experimentation, converging on a set of optimized design parameters as illustrated in Fig. 1.

A successful computer program must simulate the important physical processes underlying common applications of lasers in medicine. Therapeutic applications fall into three broad classes, depending on the physical mechanism by which the laser interacts with and alters the living tissue: photothermal, photochemical, and photomechanical. The physical processes involved in these three mechanisms include laser-light propagation, thermal heat transport, material changes such as thermal coagulation and photochemistry, and hydrodynamic motion. An introduction to many aspects of these processes can be found in a recently published textbook.[1] We have recently developed a computer program named LATIS (laser–tissue interaction) to model realistically these fundamental physical processes. This provides a tool that can be used to predict accurately and to analyze laser–tissue interaction experiments and can be used in the design process shown in Fig. 1.

In this paper we present the structure and contents of the LATIS program. We present a brief discussion of several applications and a detailed discussion of one application: the problem of laser-light dosimetry with dynamic optical properties. Similar work has been done showing the importance of dynamic optical properties during laser irradiation of biological tissues.[2]

2. LATIS Program

LATIS is a two-dimensional, time-dependent simulation program. It is based on the experience gained during 25 years of modeling high-intensity laser–matter interactions for fusion research, particularly with the LASNEX program.[3] LATIS uses cylindrical geometry, with spatial positions described by radial and axial coordinates r and z. The spatial domain of a

R. A. London, M. E. Glinsky, G. B. Zimmerman, D. S. Bailey, and D. C. Eder are with Lawrence Livermore National Laboratory, 7000 East Avenue, Livermore, California 94551. S. L. Jacques is with Oregon Medical Laser Center, Providence St. Vincent Medical Center, 9205 Southwest Barnes Road, Portland, Oregon 97225.

Received 13 February 1997; revised manuscript received 21 July 1997.

0003-6935/97/349068-07$10.00/0

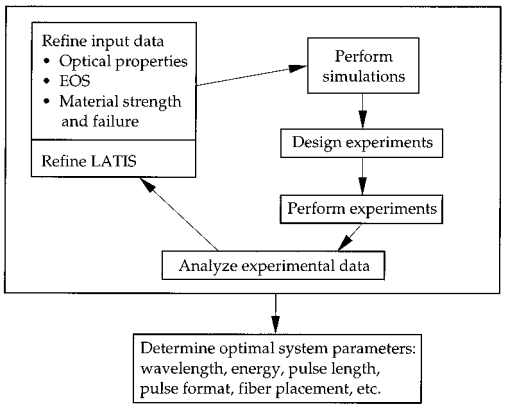

Fig. 1. LATIS used in an iterative method along with experiments to design a laser-medicine system. The cycle eventually converges on optimized design parameters.

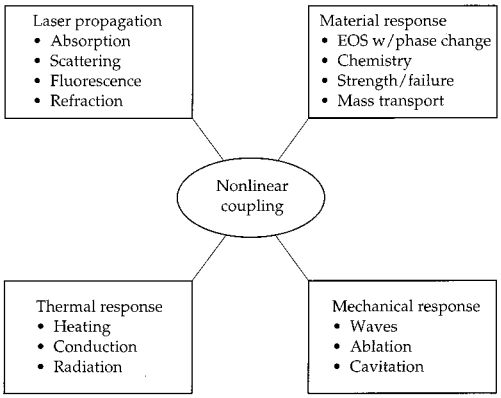

Fig. 2. LATIS models laser–tissue interactions considering four areas of coupled physical processes. Features such as the hydro response are being developed for future use in tissue ablation applications.

calculation is defined by a connected mesh of line segments containing quadrilateral zones. Each line segment intersection is called a mesh point. Positions and velocities are defined at the mesh points, while most material properties, such as temperature and density, are defined at the zone centers. Physical properties are mathematically modeled by analytic formulas, table interpolations, and both ordinary and partial differential equations. Partial differential equations are solved by finite-difference or finite-element methods. In addition, the Monte Carlo method is also used for laser transport, as described below. LATIS is written in FORTRAN and controlled by a computer science back plane called Basis.[4] Basis is an interpreter that allows the user considerable flexibility in setting up problems, adding user-defined functions without recompiling the code, and mathematical and graphical postprocessing. LATIS runs on UNIX workstations and supercomputers. A typical run time for the simulations discussed in Section 3.A is a few minutes on an HP-735 workstation.

The physical processes considered by LATIS are grouped into four categories, as illustrated in Fig. 2 and discussed below: laser propagation, thermal response, material response, and hydro response.

A. Laser Propagation

For most applications, laser propagation is calculated in the radiation-transfer approximation, although for certain situations, such as ultrashort laser pulses, a wave treatment is needed. In Ref. 1 the radiation transfer approximation in the context of laser–tissue interaction and the associated calculational methods are described. In LATIS we mainly use the time-dependent Monte Carlo method, in which light is represented by a finite number of "superphotons," typically 10^3–10^4, each representing many real photons. For example, a typical photothermal problem involves of the order of 1 J of laser energy per time step, with several hundred time steps required per simulation. In this case each superphoton represents approximately 10^{15} real photons. Henceforth we refer to the superphotons simply as photons. Propagation of the photons is treated in a probabilistic manner. In LATIS, laser photons are created along one or several line segments of the numerical mesh with spatial and angular distributions of energy specified to model light delivery devices such as end-emitting and diffusing optical fibers and focusing lenses. A fixed number of photons is introduced at the first time step of the simulation. The photons are then tracked time dependently through the spatial domain of the calculation. Fresnel reflection and refraction are calculated as photons cross material interfaces with unequal indices of refraction, such as an air–tissue interface. Scattering is calculated probabilistically along a photon's path according to the scattering coefficient, which may vary in space and time. An anisotropic angular phase function is used to select the scattering angle. We currently use the Henyey–Greenstein phase function,[5] which has been found to be a good approximation to tissue scattering.[6] Absorption is calculated analytically along each photon path according to the local absorption coefficient, without destroying the photons. The energy absorbed along the photon path is tabulated in spatial zones, where it is added to the material internal energy. Each photon carries a weight, which decreases with absorption. When the weight drops below a specified value, typically 1%, the photon is retired from the Monte Carlo calculation, and the remaining energy is deposited locally. At the end of a time step a number of photons are still alive within the spatial domain of the simulation, and a number will have been removed, either because they left the spatial domain or because their weight dropped below the minimum allowed value. If the laser source is still turned on at the beginning of the next time step, new photons are injected. In cases involving relatively long pulses (and therefore long time steps), no photons remain alive at the end of a time step: they will have been either completely absorbed or traveled out of the problem. In this case, new source photons are created at the beginning of

the next time step with the same, user-defined, number as for the first time step. For very short time steps associated with very short laser pulses, typically in the subnanosecond regime, a significant number of photons may be alive at the end of the time step. In this case, the total energy of the living photons is included with source energy in determining the average photon weight for the next time step. Underweight photons are statistically eliminated to keep the total number equal to the user-defined value.

In addition to the Monte Carlo method we have the ability to invoke the diffusion approximation for laser transport, which is generally faster but not as accurate near the surface of the material and for complicated geometries. For ultrashort pulses we are adapting a wave equation solver to calculate the laser propagation and absorption.[7] This is necessary because the absorption occurs by way of an evanescent wave extending into a high-density plasma, which cannot be described in the radiation transfer approximation.

B. Thermal Response

Absorption of the laser light primarily goes into raising the tissue temperature according to its specific heat. (For soft tissues this quantity is approximately that of water.) Heat is then carried away from the laser deposition region by thermal conduction and other processes. This is modeled with the well-known bioheat equation, essentially a diffusion equation with cooling and heating terms due to blood perfusion and boundary effects.[8,9] The effects of blood perfusion are important for relatively long pulses (>1 s), which are used mainly for photothermal therapies. Heat exchange between blood and tissue occurs most effectively in the smallest vessels (arterioles, venules, and capillaries). In these vessels the blood and tissue reach the same temperature rapidly. In larger vessels, there is little heat transfer between the blood and the tissue owing to the rapid flow rate and lower surface-to-volume ratio. Because the small vessels are generally short (≈1 mm or less) compared with other scales of interest, such as the laser spot size or the size of a desired coagulation region, the blood perfusion thermal effects are assumed to be local. By further assuming that the blood coming into the arterioles has a temperature equal to the body core temperature (37 °C), we represent the blood–tissue exchange as local heating and cooling rates that are linear in temperature and that drive the tissue toward body temperature. In the models discussed below, we assume specific temperature and damage dependence to the blood perfusion, representing increases due to vessel dilation at slightly elevated temperatures and a decrease due to coagulation at long exposures to high temperature.

C. Material Response

The material response portion of the LATIS simulation includes calculation of the equation of state (EOS) that specifies the internal energy and pressure of a material as functions of the density and temperature. We usually use steady-state, equilibrium models; however, time-dependent models can be incorporated. It is important to describe accurately phase changes in the EOS, such as the liquid–vapor change in water. In the primary implementation an EOS is generated in the form of a table and placed in a simple library format for easy access by LATIS. The tables are produced by the Livermore EOS generator, quotidian EOS (HQEOS),[10,11] which is a global model including solid, liquid, vapor, and plasma states over a wide range of temperatures and densities. We also have the ability to incorporate other models such as the National Institute of Standards and Technology steam tables.[12] Models for chemical processes, such as protein denaturation and tissue coagulation, are included. We have implemented an Arrhenius model, which describes such chemical processes by a single temperature-dependent rate equation.[13] Henceforth these processes are generically called damage. The rate equation is integrated to give a damage integral,

$$\Omega = \int k \mathrm{d}t, \tag{1a}$$

where the damage rate is

$$k = \frac{k_b T}{h} \exp\left(\frac{\Delta S}{R} - \frac{\Delta H}{RT}\right). \tag{1b}$$

In Eqs. (1a) and (1b), k_b, h, and R are the Boltzmann, Planck, and gas constants, T is temperature, and ΔS and ΔH are the entropy and enthalpy of the reaction. Equation (1a) applies formally only to ideal first-order reactions. Although in reality the damage processes in tissue are likely to be more complicated, we still use Eqs. (1) as a convenient fitting formula for experimental data for such highly temperature-sensitive reactions. The undamaged fraction of the tissue is $f_u = \exp(-\Omega)$, while the damaged fraction is $f_d = 1 - f_u$. The damage integral is used to alter both the blood perfusion and the scattering coefficient. Other chemical processes, such as those responsible for tissue fusion in a welding procedure or photochemical processes during photodynamic therapy, can be modeled in a similar manner.

Another set of important material properties are the strength and failure characteristics under mechanical forces. We currently use simple prescriptions, such as a stress–strain relation, but more sophisticated time-dependent models are under development.

D. Hydrodynamic Response

The fourth category of physical process considered by LATIS is the hydrodynamic response of the tissue. These effects include acoustic waves, elastic and plastic deformations, and large motions such as cavitation and ablation. LATIS solves partial differential equations describing mass and momentum conserva-

tion by using the Lagrangian method. In this method the spatial zones represent small mass elements. The mesh points move in response to pressures generated in neighboring zones. The mass stays in each zone, moving with the mesh. The hydrodynamic equations are solved by a finite-difference method and advanced in time by a second-order differencing scheme. The method is explicit, so that a maximum time step is set by a numerical stability criterion (the Courant limit). Other criteria, such as changes in the temperature and density, are also used to set a maximum time step to ensure an accurate and stable solution of the hydrodynamic and dynamic optics equations.

E. Coupling

The four areas of interactions are all coupled together allowing for nonlinear effects, such as alteration of the optical and thermal properties by time-dependent variations of temperature. This coupling is done explicitly by the operator splitting method, in which the time advance of each process is calculated with the most recent data from the other processes. The accuracy of this procedure is fixed with time step controls, ensuring a converged solution.

3. Applications of LATIS

A. Overview

To date, LATIS has been used to simulate both photothermal and photomechanical laser–tissue interactions. Photochemical applications are planned for future work in the areas of cancer and arthritis treatment. In the photothermal area, we have used LATIS to study the effects of dynamic optical properties on laser dosimetry[14] (which we summarize below as a detailed example of LATIS in action), the welding of intravascular patches,[15,16] and the thermal environment for general tissue welding.[17] In the photomechanical area we have applied LATIS to study high-precision tissue ablation with ultrashort pulses[18] and laser thrombolysis for stroke therapy.[19]

B. Laser Dosimetry With Dynamic Optics

Many laser applications are based on raising the temperature of a localized region of tissue for a certain period of time to cause necrosis or other alterations, such as tissue fusion. In these photothermal applications the local energy dose (energy per unit mass) delivered to the tissue is a critical parameter.

Dynamic optics is defined as the alteration of tissue optical properties by laser irradiation. The effects of dynamic optics on the total dose to the tissue, the size of the damaged region, and the reflected light pattern are important for photothermal applications of lasers, such as tumor treatments.[20] In this section we illustrate the application of LATIS to a problem in which the laser scattering coefficient and the blood perfusion change due to thermal damage. We focus on the size of the damage region, and we study how dynamic optics effects vary with the laser irradiation and tissue parameters.

We chose characteristic, but generic, tissue properties to demonstrate the capabilities of LATIS and to illustrate the physical effects involving dynamic optics. The optical properties were those of dog myocardium at a laser wavelength of 630 nm.[21] The dynamic scattering coefficient was a linear combination of an undamaged and a damaged coefficient: $\mu_s = \mu_u f_u + \mu_d f_d$, where the tissue fractions f_u and f_d are calculated as described following Eq. (1). The scattering coefficients were $\mu_u = 50\ \mathrm{cm}^{-1}$ and $\mu_d = 350\ \mathrm{cm}^{-1}$. The absorption coefficient was fixed at $\mu_a = 0.3\ \mathrm{cm}^{-1}$. Such parameters are also typical of many other soft tissues in the 630–800-nm range. Thermal properties (heat capacity and conductivity) were taken to be those of water, accurate to 30% for most tissues.[20] Damage rate coefficients were fit to average data for whitening of several tissues: dog prostate, dog heart, and rat and pig liver. The coefficients used in Eq. (1) were $\Delta S = 68.2\ \mathrm{cal\ deg}^{-1}\ \mathrm{mol}^{-1}$ and $\Delta H = 45.79\ \mathrm{kcal\ mol}^{-1}$. With these coefficients the damage time scale $(1/k)$ varies rapidly with temperature from 100 s at 65 °C to 0.5 s at 90 °C. In the simulations the temperature was kept near 72.5 °C, at which the damage time scale was 20 s. We also included temperature and damage effects on the blood perfusion using

$$P = P_0 f(T) \exp(-\Omega), \tag{2}$$

where P_0 is the constitutive perfusion, T is local temperature, $f(T)$ is a dimensionless function that accounts for vessel dilation at slightly elevated temperatures, and Ω is the damage integral. We specify $f(T)$ to be a linear function with value unity at 37 °C and 4 at 42 °C. Above 42 °C it is constant. Equation (2) causes perfusion to increase fourfold as the temperature rises, but as coagulation develops, it is reduced to zero by the damage factor. We do not include the kinetics of the perfusion change, which Kim *et al.*[2] approximated with a time constant of 20 s.[2] This is not necessary for the rather slow heating that occurs during the 60-s time exposure of our standard case. Rapid heating, which occurs with higher irradiances, leads to a rapid rise in Ω that shuts perfusion down, making the inclusion of the perfusion kinetics also not very important.

A standard case was defined with the following parameters: laser pulse length, 60 s; laser spot size (radius), 1 mm; scattering anisotropy factor, 0.9; blood perfusion rate, $0.4\ \mathrm{mL\ g}^{-1}\ \mathrm{min}^{-1}$. The laser irradiation pattern was assumed to be circular with a constant intensity distribution, and the tissue was assumed to be initially homogeneous. The irradiation geometry and problem zoning are shown in Fig. 3. Fine zones were placed near the laser spot, where the highest resolution was desired, while coarser zones were used far from the laser spot. This zoning technique increased the problem resolution while maintaining a relatively small number of zones.

The laser intensity was controlled by a thermostat function that keeps the surface temperature of the directly irradiated region within a desired range.

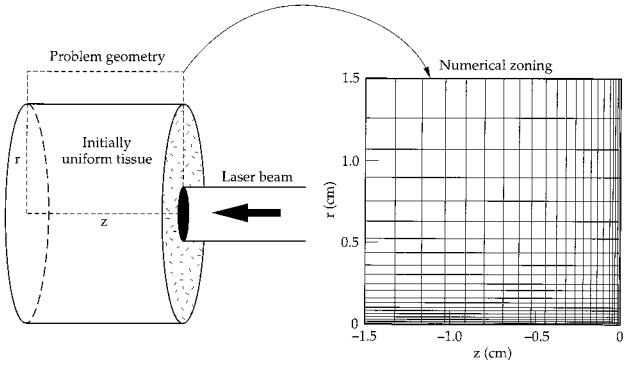

Fig. 3. Laser–tissue interaction modeled in cylindrical geometry, with fine zones near the laser spot and coarse zones far from the laser spot.

This type of control is motivated by clinical considerations, such as achieving a maximum damage rate over a specified volume without approaching temperatures near 100 °C, at which tissue dehydration might occur. We actively controlled the laser intensity by monitoring the average temperature in a 3×3 set of tissue zones within the laser spot. This treatment could easily by extended to consider a simulated diagnostic signal, such as an infrared temperature sensor. We turned the laser off when the temperature exceeded the set maximum and then turned it back on when the temperature dropped below the set minimum. We chose a minimum of 70 °C and maximum of 75 °C. For the standard case the laser power during on periods was 5 W. Figure 4 shows the time histories of the control temperature T and the total energy E delivered to the tissue. The temperature built up to the set value in 5 s. The laser power was then switched on and off with a period of ~2 s according to the thermostat function mentioned above. This technique enabled good control of the damage progress and avoided adverse effects associated with dehydration or vaporization as temperatures approached 100 °C. Such a temperature-control technique has recently been experimentally demonstrated using infrared radiometry by several groups.[23–25]

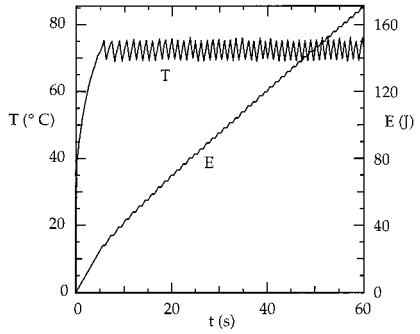

Fig. 4. Temperature controlled to a desired range by turning the laser power on and off as illustrated by the temperature and laser energy histories for the standard case.

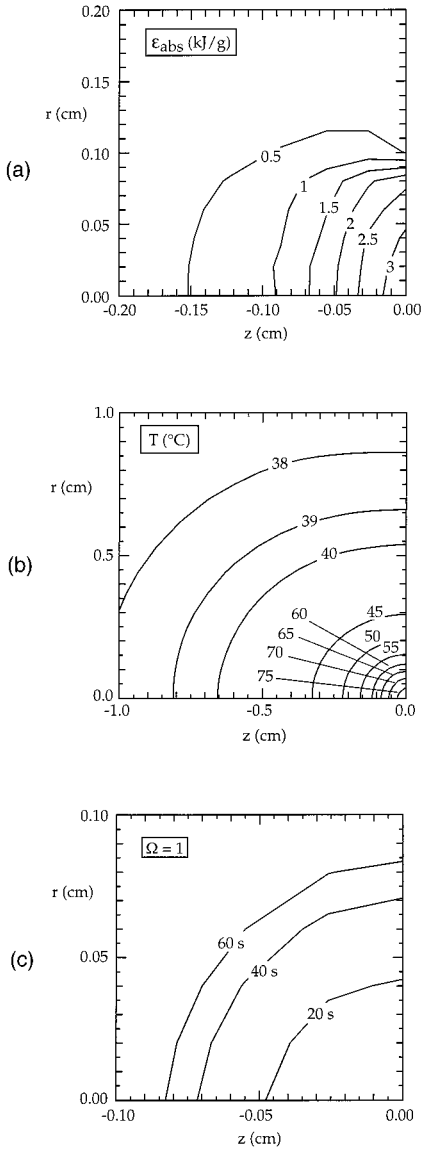

Fig. 5. (a) Total absorbed energy density integrated over the 60-s pulse. Laser and tissue conditions are for the standard case. This pattern reflects the light distribution. (b) The resultant temperature distribution at 60 s shows the conductive spreading relative to the absorbed energy. (c) Damage region ($\Omega = 1$) is shown at various times during the pulse. It grows because of both heat diffusion and time for accumulation of damage.

Results for the distribution of absorbed laser energy, temperature, and damage integral for a simulation of the standard case are shown in Fig. 5. The absorbed laser light reflects the time-average light distribution, since the absorption coefficient is constant. Owing to heat diffusion the temperature distribution extended further from the laser focal region than the laser deposition. The size of the damage zone, as indicated by the $\Omega = 1$ contours of Fig. 5(c), grew in time, because of both heat diffusion beyond the energy deposition region and the increasing time for accumulation of damage.

We now compare the damage zone ($\Omega \geq 1$) for the standard case with dynamic optics with that with

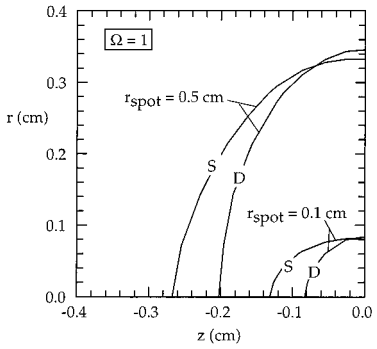

Fig. 6. Size of the damage regions reduced by dynamic optics, as shown for the standard case and for a case with a large spot. The effect of dynamic optics is greater for the standard spot than for the large spot. All curves are for the end of the pulse (at 60 s).

static optics in Fig. 6. By static optics we mean a simulation in which the scattering coefficient was kept fixed at its undamaged value even though the tissue became damaged. It is clear that the inclusion of dynamic optics reduces the size of the damage zone. To measure this reduction we defined a damage ratio as the depth of the damage zone at $r = 0$ with dynamic optics relative to that without dynamic optics:

$$D \equiv \frac{z(\Omega = 1)\text{dynamic}}{z(\Omega = 1)\text{static}}. \tag{3}$$

For the standard case ($r = 0.1$ cm), as shown in Fig. 6, we found $D = 0.63$. For a larger spot size ($r = 0.5$ cm), also shown in Fig. 6, the effect of dynamic optics was somewhat less than for the standard case, $D = 0.76$.

We performed a parametric study that quantified the reduction in the damage zone caused by dynamic optics. For each parameter set, we performed two simulations: one with dynamic optical coefficients and one with static coefficients. We then formed the damage ratio as defined above. The parameter variations and resultant damage ratios are listed in Table 1.

The variation with spot size is the greatest. It can be understood by comparing the spot size to the diffusive optical penetration depth $\delta = [3\mu_a(\mu_s' + \mu_a)]^{-1/2}$, where μ_s' is the reduced scattering coefficient, $' \equiv \mu_s(1 - g)$. For the undamaged tissue, $\delta = 0.46$ cm; for the damaged tissue, $\delta = 0.18$ cm. For spot sizes larger than δ (the case of a 0.5-cm spot size), the deposition region is properly given by δ, which scales as $\mu_s'^{-1/2}$ for $\mu_s' \gg \mu_a$ as in the case. For small spot sizes the laser light scatters out of the beam, leading to a smaller deposition region, scaling approximately as $\mu_s'^{-1}$. This higher dependence on μ_s leads to the relatively larger effect of dynamic optics for the smaller spots. The variation with pulse length stems from the relationship to the typical damage time scale. We controlled the surface temperature to an average value of 72.5 °C, which gave a characteristic damage time scale of 20 s. Thus pulses of ~20 s or less do not have enough time to produce a large damage zone and therefore show less difference between the dynamic optics and the static optics cases, as indicated in Table 1. We also explored variations in the isotropy of scattering and the blood perfusion rate. The isotropic scattering case ($b = 0$) assumed smaller scattering coefficients but with the reduced scattering coefficient μ_s' kept the same as for the standard case with $g = 0.9$. This was found to have little effect on the simulation results. The case with no blood perfusion showed 10% larger damage depth in both dynamic and static cases but little differential effect, as seen in Table 1.

Table 1. Parameter Variations and Corresponding Damage Ratios

Parameter Variation	Damage Ratio
Standard case	0.63
Short pulse (20 s)	0.76
Long pulse (180 s)	0.63
Small spot (0.01 cm)	0.39
Large spot (0.5 cm)	0.76
Isotropic scattering	0.67
No blood perfusion	0.66

In summary we see that dynamic optics reduces the depth of damage by ~33% in most cases, with the greatest sensitivity to the irradiation spot size and pulse length. This study illustrates the importance of including such nonlinear effects in designing protocols for laser thermotherapies. Projects on thermotherapy for benign prostate hyperplasia and laser–tissue welding are currently in progress in which similar modeling is being used to design experiments and to compare directly with measured data.

4. Summary

The LATIS computer program is being developed to treat all the important aspects of laser–tissue interaction including laser propagation, thermal effects, material effects, and hydrodynamics, in a fully coupled manner. In LATIS we now have a powerful tool for designing new medical devices and procedures through computational simulation. LATIS is being applied to areas of photothermal therapy, tissue welding, hard-tissue ablation, and thrombolysis.

This work was performed under the auspices of the U.S. Department of Energy by Lawrence Livermore National Laboratory under contract W-7405-ENG-48.

References

1. A. J. Welch and M. J. C. Van Gemert, *Optical-Thermal Response of Laser-Irradiated Tissue* (Plenum, New York, 1995).
2. B.-M. Kim, S. L. Jacques, S. Rastegar, S. Thomsen, and M. Motamedi, "Nonlinear finite element analysis of the role of dynamic changes in blood perfusion and optical properties in laser coagulation of tissue," IEEE J. Selec. Top. Quantum Electron. **4,** 922–933 (1996).

3. G. B. Zimmerman and W. L. Kruer, "Numerical simulation of laser-initiated fusion," Commun. Plasma Phys. Controlled Fusion **11,** 51–61 (1975).
4. P. F. DuBois, "Making applications programmable," Comput. Phys. **8,** 70–74 (1994).
5. L. G. Henyey and J. L. Greenstein, "Diffuse radiation in the galaxy," Astrophys. J. **93,** 70–83 (1941).
6. S. L. Jacques, C. A. Alter, and S. A. Prahl, "Angular dependence of HeNe laser light scattering by human dermis," Lasers Life Sci. **1,** 309–333 (1987).
7. W. E. Alley, "A Maxwell equation solver for the simulation of moderately intense ultra-short pulse laser experiments," UCRL-LR-105820-92 (Lawrence Livermore National Laboratory, Livermore, Calif., 1992), pp. 160–165.
8. Y. I. Cho, ed., "Bioengineering heat transfer," in *Advances in Heat Transfer* (Academic, San Diego, Calif., 1992), Vol. 22.
9. C.-S. Orr and R. C. Eberhart, "Overview of bioheat transfer," in *Optical-Thermal Response of Laser-Irradiated Tissue*, A. J. Welch and M. J. C. Van Gemert, eds. (Plenum, New York, 1995), pp. 367–384.
10. R. M. More, K. H. Warren, D. A. Young, and G. B. Zimmerman, "A new quotidian equation of state (QEOS) for hot dense matter," Phys. Fluids **31,** 3059–3078 (1988).
11. D. A. Young and E. M. Corey, "A new global equation of state for hot, dense matter," J. Appl. Phys. **78,** 3748–3755 (1995).
12. L. Haar, J. S. Gallagher, and G. S. Kell, *NBS/NRC Steam Tables* (Hemisphere, Washington, D.C., 1984).
13. J. Pearce and S. Thomsen, "Rate process analysis of thermal damage," in *Optical-Thermal Response of Laser-Irradiated Tissue*, A. J. Welch and M. J. C. Van Gemert, eds. (Plenum, New York, 1995), pp. 561–608.
14. R. A. London, M. E. Glinsky, G. B. Zimmerman, D. C. Eder, and S. L. Jacques, "Coupled light transport–heat diffusion model for laser dosimetry with dynamic optical properties," in *Laser-Tissue Interaction VI*, S. L. Jacques, ed., Proc. SPIE **2391,** 434–442 (1995).
15. M. E. Glinsky, R. A. London, G. B. Zimmerman, and S. L. Jacques, "Modeling of endovascular patch welding using the computer program LATIS," in *Laser-Tissue Interaction VI*, S. L. Jacques, ed., Proc. SPIE **2391,** 262–272 (1995).
16. M. E. Glinsky, R. A. London, G. B. Zimmerman, and S. L. Jacques, "Computer modeling of endovascular patch welding using temperature feedback," in *Medical Applications of Lasers III*, F. Laffitte, ed., Proc. SPIE **2623,** 349–358 (1996).
17. D. J. Maitland, D. C. Eder, R. A. London, M. E. Glinsky, and B. A. Soltz, "Dynamic simulations of tissue welding," in *Lasers in Surgery: Advanced Characterization, Therapeutics, and Systems VI*, R. R. Anderson, ed., Proc. SPIE **2671,** 234–242 (1996).
18. R. A. London, D. S. Bailey, D. A. Young, W. E. Alley, M. D. Feit, A. M. Rubenchik, and J. Neev, "Computational modeling of ultra-short-pulse ablation of enamel," in *Laser–Tissue Interaction VII,* S. L. Jacques, ed., Proc. SPIE **2681,** 233–244 (1996).
19. M. Strauss, R. A. London, M. E. Glinsky, P. A. Amendt, D. J. Maitland, D. S. Bailey, D. A. Young, and S. L. Jacques, "Computational modeling of laser thrombolysis for stroke treatment," in *Lasers in Surgery: Advanced Characterization, Therapeutics, and Systems VI,* R. R. Anderson, ed., Proc. SPIE **2671,** 11–21 (1996).
20. G. Muller and A. Roggan, *Laser-Induced Interstitial Thermotherapy* (Society of Photo-Optical Instrumentation Engineers, Bellingham, Wash., 1995).
21. S. L. Jacques and M. O. Gaeeni, "Thermally induced changes in optical properties of heart," in *Proceedings of the 11th International Conference of the IEEE Engineering in Medicine and Biology* (IEEE, New York, 1989), pp. 1199–1200.
22. J. W. Valvano, "Tissue thermal properties and perfusion," in *Optical-Thermal Response of Laser-Irradiated Tissue*, A. J. Welch and M. J. C. Van Gemert, eds. (Plenum, New York, 1995), pp. 445–488.
23. T. N. Glenn, S. Rastegar, S. L. Jacques, and F. Tittel, "Finite element analysis of temperature-controlled laser coagulation of biological tissue," in *Laser-Tissue Interaction V*, S. L. Jacques, ed., Proc. SPIE **2134A,** 383–390 (1994).
24. B. Lobel, O. Eyal, E. Belotserkovsky, O. Shenfeld, N. Kariv, B. Goldwasser, and A. Katzir, "*In vivo* CO_2 laser rat urinary bladder welding with silver halide fiber optic radiometric temperature control," in *Lasers in Surgery: Advanced Characterization, Therapeutics, and Systems V,* R. R. Anderson, ed., Proc. SPIE **2395,** 517–522 (1995).
25. I. Cilesiz, E. K. Chan, A. J. Welch, and S. L. Thomsen, "Controlled temperature tissue fusion: Ho:YAG laser welding of rat intestine *in vivo*," in *Lasers in Surgery: Advanced Characterization, Therapeutics, and Systems V*, R. R. Anderson, ed., Proc. SPIE **2395,** 523–534 (1995).